Supporting Information

Lomas et al. 10.1073/pnas.1420760111

SI Text

P Uptake Rate Calculations

Whole-community and taxon-specific assimilation rates were calculated using the same equation as follows:

$$V_{P_i} = \left[\frac{\beta_{\text{sample}}}{n}\right]^{\left(\frac{\Delta T \cdot \ln 2}{\lambda}\right)} \left[\frac{1}{\beta_{T_A}}\right] \left[\frac{P}{T_o}\right],$$

where V_{Pi} is the cell-specific utilization rate (in attomoles of $^{33}P_i$ per cell per hour); β_{sample} and β_{TA} are the beta emission activities (in counts per minute) for the sorted sample and the total activity added, respectively; n is the number of cells sorted; ΔT is the elapsed time from ^{33}P isotopic tracer addition to counting; T_o is the incubation duration; λ is the decay constant of ^{33}P (half life = 25.4 d); P is the ambient concentration of the P source (in nanomoles per liter). The method detection limit following this protocol is ∼0.5 nM with a precision of ±5% at 5 nM.

Phosphate Cell Quotas

Samples for taxon-specific cellular P quota (Q_p) were collected as previously described with all samples except station 2 representing newly available data (1). Briefly, whole water samples were collected and gently concentrated on a 0.4-μm polycarbonate filter. Cells were gently resuspended, and either sorted by flow cytometry immediately or fixed with paraformaldehyde [0.5% (vol/vol) final concentration] and stored at −80 °C until they could be sorted. Once sorted, samples were filtered on 13-mm silver filters (*Prochlorococcus* and *Synechococcus*) or GF/F filters (eukaryotes) and analyzed as particulate phosphorus samples using the ash-hydrolysis method (2, 3). All samples were corrected for filter blanks. Paired comparison of unfixed and fixed cells from the same station/depth found that fixation had no effect on estimates of cellular P content (data not shown). No efforts were made to separate particulate inorganic from organic phosphorus so data are simply referred to as particulate phosphorus. For analysis, sample filters were placed in acid-cleaned [10% (vol/vol) HCl] and precombusted glass scintillation vials along with 2 mL of 17 mM $MgSO_4$, dried down at 80–90 °C, and then combusted at 500 °C for 2 h. After cooling to room temperature, 5 mL of 0.2 M HCl was added to each vial and hydrolyzed at 80 °C for 30 min. After cooling to room temperature, soluble reactive phosphate mixed reagent was added (4), sample was clarified by centrifugation, and absorbance was read at 885 nm. Samples were calculated against a potassium monobasic phosphate standard. Oxidation efficiency and standard recovery was tested with each sample run using an ATP standard solution and a certified phosphate standard (Ocean Scientific International; Phosphate Nutrient Standard Solution). In our laboratory, the precision of this method is ∼9% at 2.5 nmol of P in the sample, and ∼1% at 15 nmol of P in the sample. The method detection limit, defined herein as three times the SD of the lowest standard (2.5 nM) is ∼0.1 nmol·L^{-1}.

Biodiversity Uptake Model with Adaptation and Acclimation

Model Design. The Droop model links cell growth rates to the internal content of the most limiting nutrient (5). If Q represents the cell quota for such limiting nutrient (in moles per cell), the growth rate μ (per day) follows the equation:

$$\mu(Q) = \mu_{\max} \frac{\left(1 - Q_{\min}/Q\right)}{\left(1 - Q_{\min}/Q_{\max}\right)},$$

where $Q_{\max}$ represents the maximum value for the quota (related to the maximum storage capacity of the cell), and $Q_{\min}$ is the minimum nutrient content required for growth. Note that we chose a normalized version of the model (6), with which we ensured that the parameter $\mu_{\max}$ expresses the (measurable) maximum value of the growth rate when Q reaches its maximum possible value. The cell quota, in turn, changes with time following a simple balance equation:

$$\frac{dQ}{dt} = V_{Pi} - \mu(Q)Q,$$

where V_{Pi} represents uptake rate (in attomoles per cell per hour). On the other hand, P_i uptake rate satisfies a Michaelis–Menten functional dependence as follows:

$$V_{P_i} = \frac{V_{\max} P_i}{P_i + K_{\text{eff}}},$$

through which V_{Pi} depends on phosphate concentration, P_i, following a hyperbolic function modulated by the kinetic parameters, $V_{\max}$ and K_{eff}. The latter represents a diffusion-limitation correction that takes into account that the cell may develop a boundary layer due to the very low phosphate concentrations typical for the western North Atlantic Ocean (7):

$$K_{\text{eff}} = K_S + \frac{V_{\max}}{4\pi\, D_{P_i} r_{\text{cell}}},$$

where r_{cell} is cell radius (in decimeters) and D_{Pi} (in square decimeters per second) is the diffusivity constant for the focal resource (7). The dynamics of the population are represented by the simple equation:

$$\frac{dB}{dt} = (\mu(Q) - m)B,$$

where B is the number of cells in the population, and m encodes any source of mortality for phytoplankton (per day).

Next, we consider phytoplankton acclimation abilities by using an equation that links the change in time of the maximum uptake rate, $V_{\max}$, to the nutritional state of the cell (i.e., its quota) (7). Through this equation, the dynamics of $V_{\max}$ (i.e., changes in the number of uptake proteins) depend on the internal content of the nutrient and, by extension, on the nutritional history of the cell. Thus, cells regulate the number of proteins in response to quota changes: when Q is low, the cell up-regulates the synthesis of such proteins to increase the absorbing area of the cell, thereby increasing the uptake rate; on the other hand, quotas close to the maximum storage limit allow the cell to down-regulate protein production and save associated synthesis and maintenance energy (7). All this phenomenology can be modeled, at the population level, using the following equation (7, 8):

$$\frac{dV_{\max_B}(t)}{dt} = k_2 \left[\nu H(1 - A_{\text{rel}}(t)) F\left(\frac{Q_{\max} - Q(t)}{Q_{\max} - Q_{\min}}\right)\right] - mV_{\max_B}(t),$$

where $V_{maxB} = B \cdot V_{max}$. H is a Heaviside function that introduces a limit to the maximum number of uptake proteins for the cell, set by the cell's surface area, with A_{rel} the ratio of absorbing to total cell area (which, therefore, depends on the number of proteins). k_2 is the assimilation rate (inverse of the handling or assimilation time):

$$k_2 = 4\pi D_{P_i} r_{site},$$

r_{site} is the absorbing radius of an uptake protein, and ν is the maximum number of sites produced per unit time. $F(x) \in [-1, 1]$, is a sigmoid function, defined here as follows:

$$F\left(\frac{Q_{max} - Q}{Q_{max} - Q_{min}}\right) = \frac{2}{1 + e^{-k_F\left(\frac{Q_{max} - Q}{Q_{max} - Q_{min}}\right)}} - 1.$$

k_F is a shape factor. The choice of F is justified because protein synthesis is the result of gene expression, typically represented by sigmoid functions (e.g., Hill function); however, other functional forms with similar Q dependence do not alter the qualitative behavior of the ecological model (7).

Finally, we set chemostat conditions in which we altered the dilution rate, w (per day), to represent different locations. Thus, the dynamics for the resource concentration, P_i (in nanomoles per liter) are given by the following:

$$\frac{dP_i}{dt} = w(P_{i0} - P_i) - V_{Pi} B,$$

where P_{i0} is a (fixed) input of nutrient that can be tuned in chemostats.

Size-Based Parameterization. We considered size as the master trait representing phytoplankton strains. Thus, we chose a size-based parameterization; if s is cell size (or volume, in cubic micrometers), we can express the allometric relationship for Q_{min}, Q_{max}, or ν generically as $X = a_X s^{bX}$ and used the across-taxon allometries proposed for phosphorus (9, 10). In addition, we devised an allometry for the parameter ν that ensured that the qualitative behavior expected for V_{max} against P_i, relative to that of V_{Pi} [e.g., both should converge for high P_i (8, 11)], was observed regardless of cell size.

These allometries sufficed to find a qualitative agreement with our observations. To also reach a quantitative agreement, we needed to make use of the wide ranges provided in (9) for a_K, b_K, a_μ, and b_μ. This approach was justified by the fact that each taxon should be really represented by its own specific allometry for each trait. In this way, we assumed that eukaryotes shared an allometry for K_s (specifically, $a_K = 2.00$ nM, $b_K = 0.56$), different from that of Cyanobacteria ($a_K = 3.98$ nM, $b_K = 0.3$). Note that this choice stretched the value of the coefficients a_K considerably beyond the limits obtained previously (9). Still, our selected coefficients and exponent ensured that smaller cells (Cyanobacteria) showed smaller K_s than bigger cells (eukaryotes). Similarly, we used $b_\mu = -0.2$ for eukaryotes and $b_\mu = -0.3$ for prokaryotes. Finally, we assumed that lineages were represented by different a_μ. Thus, we tuned the latter parameter to identify the emergent trait values for each lineage (Table S2).

Model Evaluation. To replicate the observed P_i uptake kinetics curves (Fig. 1), we focused on each taxon separately. Our assumption was that the biggest contribution to the measured taxon-specific curves arose from the dominant within-taxon strain in each location. Thus, we used the model described above to calculate the most competitive strain for a fixed value of a_μ, varying the dilution rate (that is, resource concentration) to replicate different locations. Furthermore, we used three different methods to calculate the most competitive strain for each of those locations.

For the first method, we initialized our system by randomly assigning sizes ranging from 10^{-3} to 10^8 μm^3 to 300–500 ecotypes, aiming at representing any possible within-taxon variability. Then, we let them compete for the single available resource. According to expectations, only one winner was observed per location. We used several replicates to obtain the characteristic winner of each location, due to the stochastic nature of the initial condition. The second method was devised to obtain the pairwise invasibility plot (PIP) for each location (Fig. S7*A*). PIPs allow one to identify whether the strain is a local or a global winner in the trait space (12). Thus, we confronted a resident strain of size s with an immigrant strain of size s', and let them compete until one single winner was observed. The process was then repeated sweeping all possible combinations of s and s' within specific ranges. Thus, we confirmed the results of the previous analyses, obtaining in all cases (global) winner's sizes in agreement with the previous simulations (Fig. S7*A*). The third method considered evolution explicitly by using an eco-evolutionary framework (13). Starting from a random strain, new mutant strains are introduced according to the dynamics of the population and a fixed mutation rate. Competition for resources makes strains disappear; mutation and extinction allow the population to explore the trait space in a continuous way until the most competitive trait value is present. Due to its competitive advantage, this strain grows and resists invasion by any other strain. Thus, the average trait value for the population remains stable around the most competitive strain's trait value—i.e., the evolutionarily stable strategy (ESS). Using this framework, the resulting ESS matched the sizes obtained with the other two methods above (Fig. S7*B*). As an important additional result, the emergent V_{max} dependence on the size of the winning ecotypes shared, for all four lineages explored through simulations, a similar exponent $b_{Vmax} \sim 1$.

Finally, to replicate the variation in V_{max} observed under conditions of different phosphate availability (Fig. 3), we used the same model and allometries described above but setting a fixed characteristic size representing each lineage. More specifically, we used $s = 0.1$ μm^3 for *Prochlorococcus* and $s = 20$ μm^3 for eukaryotes. Then, we quantified the kinetic parameters V_{max}, K_s, and their ratio, α, resulting from the different stationary states (i.e., different nutrient conditions) obtained with chemostat environments varying the dilution rate, w (Fig. S5).

Model with No Regulation of Transport Proteins (i.e., Only Adaptation). To discern to what extent the combination of adaptation (evolutionary changes in cell size and, therefore, in size-related traits) and acclimation (regulation of transporters) was responsible for the observed patterns, we used a more simplistic approach in which we suppressed acclimation in the model above by keeping V_{max} constant. This approach was, thus, not able to replicate the kinetic curves.

Assuming that $dV_{max}/dt = 0$, we could use an allometry to initialize a constant V_{max}. We assumed $a_{Vmax} = 33.08$ amol·cell^{-1}·h^{-1}, and $b_{Vmax} = 1$ (9). This simplification allowed us to obtain an explicit expression for the population growth rate and the ESS for size. By definition, the per-capita growth rate is given by the following:

$$\lambda = \frac{1}{B}\frac{dB}{dt} = \mu - m.$$

By solving for stationary state, the quota dynamic equation, we obtain the following:

$$Q^* = \frac{V_{max}(Q_{max} - Q_{min})P_i^* + \mu_{max} Q_{min} Q_{max}(P_i^* + K_S)}{\mu_{max} Q_{max}(P_i^* + K_S)},$$

and, replacing the expression above into the population growth rate:

$$\lambda = \frac{\mu_{\max} V_{\max} Q_{\max}}{V_{\max}(Q_{\max} - Q_{\min}) + \mu_{\max} Q_{\max} Q_{\min}} + \frac{P_i^*}{P_i^* + \left(\frac{\mu_{\max} Q_{\max} Q_{\min} K_S}{V_{\max}(Q_{\max} - Q_{\min}) + \mu_{\max} Q_{\max} Q_{\min}} \right)} - m = \mu_{\max_M} \frac{P_i^*}{P_i^* + \kappa} - m.$$

Thus, the population growth rate can be expressed as a Monod-like growth rate (14), with parameters given by the following:

$$\mu_{\max_M} = \frac{\mu_{\max} V_{\max} Q_{\max}}{V_{\max}(Q_{\max} - Q_{\min}) + \mu_{\max} Q_{\max} Q_{\min}},$$

$$\kappa = \frac{\mu_{\max} Q_{\max} Q_{\min} K_S}{V_{\max}(Q_{\max} - Q_{\min}) + \mu_{\max} Q_{\max} Q_{\min}}.$$

The population growth rate can subsequently be used as invasion fitness. Therefore, the ESS is the point where the lines for $\lambda = 0$ cross in a PIP (i.e., considering a resident and an invading phenotype; see above). The ESS is also a point where the resident's fitness reached a maximum (12) and fulfills the following:

$$\left. \frac{\partial \lambda}{\partial s} \right|_{P_i = P^*_{i\ res}} = 0,$$

$$\left. \frac{\partial^2 \lambda}{\partial s^2} \right|_{P_i = P^*_{i\ res}} < 0.$$

As a consequence, we can use the expression above to numerically estimate the size of the most competitive sizes within a taxon (i.e., fixed a_μ), for a variety of environments (i.e., for several w). Note that this simple model could not replicate quantitatively the observed patterns even although the allometry used for $V_{\max}$ is similar to that emerging from the complete model. Parameterizing this simpler model to replicate observations quantitatively involved fine-tuning most of the available allometric coefficients. In contrast, observed values emerged from the complete model by acknowledging essential functional differences between eukaryotes and Cyanobacteria (affecting here the allometry for K_s), and using a_μ as a taxon-specific parameter. In addition, the complete model allowed us to replicate the observed behavior for the kinetic parameters, also within realistic ranges. This discrepancy highlights the important role of acclimation in creating those patterns.

In summary, although this simple model and calculations showed that adaptation could be responsible for the qualitative shape of the uptake curves, only a combination of adaptation and acclimation was able to fully explain all of the observed phenomenology.

Other Model Options. We also tried more phenomenological implementations of acclimation, such as replacing $V_{\max}$ by the following (15, 16):

$$V_{\max} = V^{\text{hi}}_{\max} \left(\frac{Q_{\max} - Q}{Q_{\max} - Q_{\min}} \right),$$

or a generalization of the above (8, 11):

$$V_{\max} = V^{\text{hi}}_{\max} - \left(\frac{Q - Q_{\min}}{Q_{\max} - Q_{\min}} \right) \left(V^{\text{hi}}_{\max} - V^{\text{lo}}_{\max} \right),$$

where the superscript "hi" and "lo" refer to the value of the maximum uptake rate for low and high P_i, respectively. The two expressions above showed an ultimate dependence of $V_{\max}$ on resource concentration qualitatively similar to that emerging from the mechanistic model used in the main text and observed in the data (i.e., $V_{\max}$ decreasing with P_i). Unfortunately, although these expressions allowed for analytical solutions in the spirit of that presented in the previous section, none of them were able to replicate both qualitatively and quantitatively the behavior for uptake and kinetic parameters described in the main text. Thus, only a mechanistic implementation of such acclimation could reproduce the mentioned observations.

1. Martiny AC, et al. (2013) Strong latitudinal patterns in the elemental ratios of marine plankton and organic matter. *Nat Geosci* 6(4):279–283.
2. Solorzano L, Sharp JH (1980) Determination of total dissolved phosphorus and particulate phosphorus in natural-waters. *Limnol Oceanogr* 25(4):754–757.
3. Lomas MW, et al. (2010) Sargasso Sea phosphorus biogeochemistry: An important role for dissolved organic phosphorus (DOP). *Biogeosciences* 7(2):695–710.
4. Parsons TR, Maita Y, Lalli CM (1984) *A Manual of Chemical and Biological Methods for Seawater Analysis* (Pergamon, Oxford).
5. Droop MR (1968) Vitamin B12 and marine ecology. IV. The kinetics of uptake, growth and inhibition in Monochrysis lutheri. *J Mar Biol Assoc U K* 48(3):689–733.
6. Flynn KJ (2008) Use, abuse, misconceptions and insights from quota models—the Droop cell quota model 40 years on. *Oceanogr Mar Biol Annu Rev* 46(46):1–23.
7. Bonachela JA, Raghib M, Levin SA (2011) Dynamic model of flexible phytoplankton nutrient uptake. *Proc Natl Acad Sci USA* 108(51):20633–20638.
8. Bonachela JA, Allison SD, Martiny AC, Levin SA (2013) A model for variable phytoplankton stoichiometry based on cell protein regulation. *Biogeosciences* 10(6): 4341–4356.
9. Edwards K, Thomas M, Klausmeier CA, Litchman E (2012) Allometric scaling and taxonomic variation in nutrient utilization traits and maximum growth rate of phytoplankton. *Limnol Oceanogr* 57(2):554–566.
10. Grover JP (1989) Influence of cell shape and size on algal competitive ability. *J Phycol* 25(2):402–405.
11. Morel FMM (1987) Kinetics of nutrient uptake and growth in phytoplankton. *J Phycol* 23(1):137–150.
12. Dercole F, Rinaldi S (2008) *Introduction to Analysis of Evolutionary Processes: The Adaptive Dynamics Approach and Its Applications* (Princeton Univ Press, Princeton).
13. Bonachela JA, Levin SA (2014) Evolutionary comparison between viral lysis rate and latent period. *J Theor Biol* 345:32–42.
14. Monod J (1950) La technique de culture continue theorie et applications. *Ann Inst Pasteur (Paris)* 79:390–410.
15. Geider RJ, MacIntyre HL, Kana TM (1998) A dynamic regulatory model of phytoplanktonic acclimation to light, nutrients, and temperature. *Limnol Oceanogr* 43(4):679–694.
16. Verdy A, Follows M, Flierl G (2009) Optimal phytoplankton cell size in an allometric model. *Mar Ecol Prog Ser* 379:1–12.

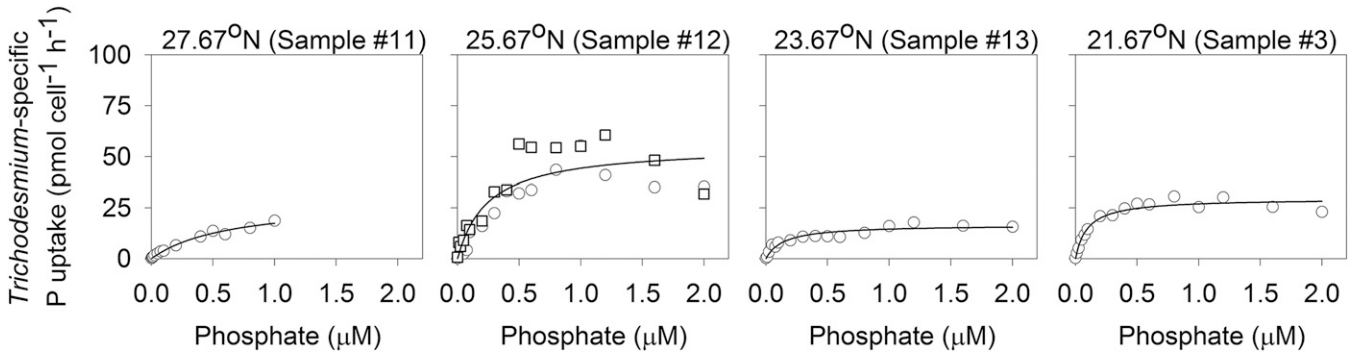

Fig. S1. Phosphate uptake kinetics for the N_2 fixer *Trichodesmium* across the western North Atlantic Ocean.

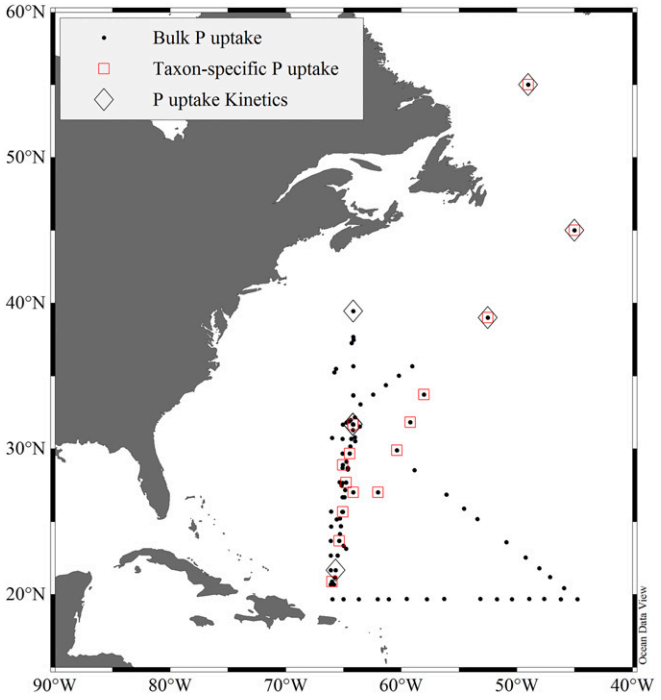

Fig. S2. Map of samples used in this study, collected over multiple cruises led by Lomas in the western subtropical North Atlantic Ocean. This includes samples for P_i uptake kinetics, in situ uptake rates for the whole community as well as specific population, and other factors (particulate phosphate, dissolved inorganic phosphate, and P cell quota for specific populations). The taxon-specific P_i uptake data from two of the six cruises were previously published in Casey et al. (1).

1. Casey JR, et al. (2009) Phytoplankton taxon-specific orthophosphate (Pi) and ATP utilization in the western subtropical North Atlantic. *Aquat Microb Ecol* 58(1):31–44.

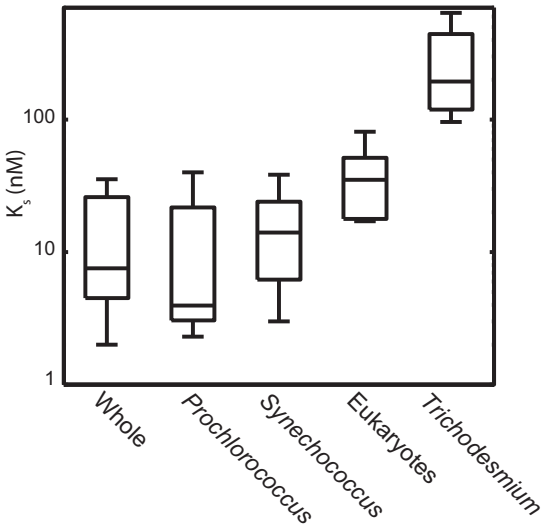

Fig. S3. Phosphate uptake half-saturation concentrations (K_s) for the whole community and specific phytoplankton groups. The line in the box represents the median, the box represents the 25th and 75th percentiles, and the whiskers cover ~99.3% of the data. K_s values are significantly different between groups (one-way ANOVA, $P < 0.05$).

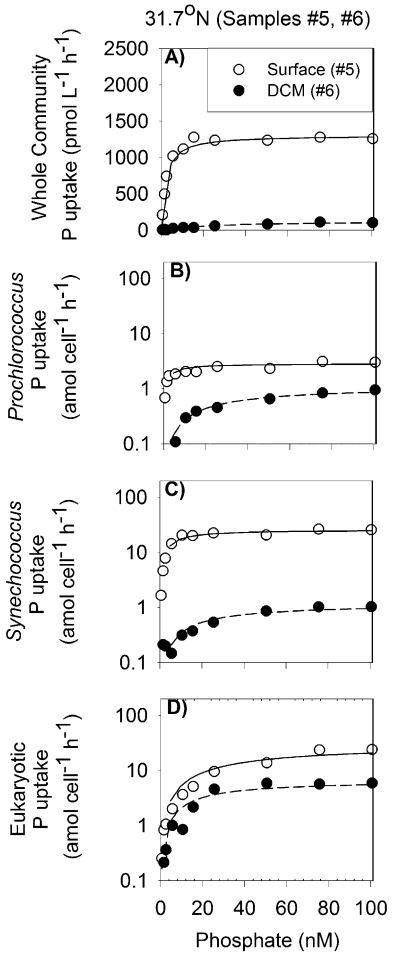

Fig. S4. Comparison of the P_i uptake kinetics for the whole community (*A*) as well as *Prochlorococcus* (*B*), *Synechococcus* (*C*), and eukaryotic phytoplankton (*D*) populations between surface and deep chlorophyll maximum (DCM).

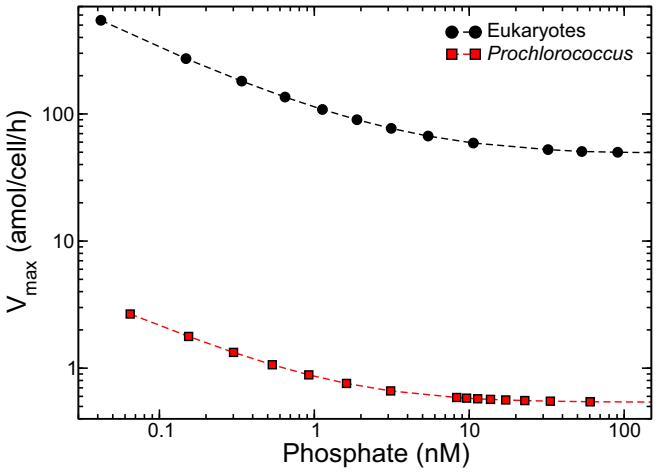

Fig. S5. Eco-evolutionary model prediction for V_{max}. The predictions are for *Prochlorococcus* and eukaryotic phytoplankton as a function of ambient P_i concentrations.

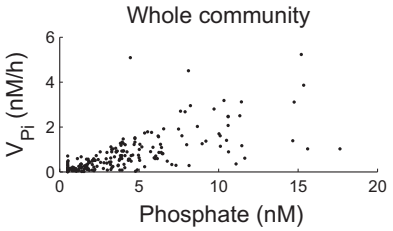

Fig. S6. In situ P_i uptake rates for the whole community. The samples are taken across the western North Atlantic Ocean region (n = 250) at depths less than 50 m. The solid line represents a simple linear regression with an intercept = 0.

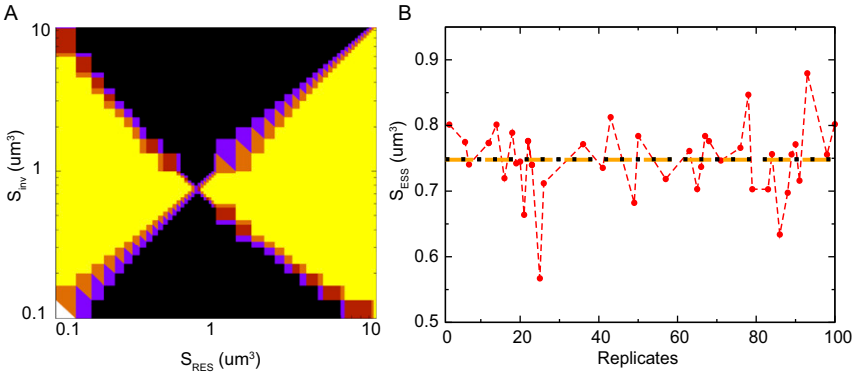

Fig. S7. Biodiversity model evaluations. (*A*) Pairwise invasibility plot (PIP) obtained with the evolutionary model that includes acclimation, with a *Synechococcus* parameterization and w = 0.5; yellow regions indicate values of resident S_{RES} and invader S_{inv} sizes for which the resident is outcompeted, whereas the resident resists invasion in the black regions. (*B*) Evolutionarily stable strategy (ESS) obtained with the eco-evolutionary framework with a *Synechococcus* parameterization and w = 0.5; for all of the different replicates of the numerical simulation, the reached ESS coincides with that obtained with the PIP.

Table S1. Whole-community and population-specific phosphate uptake kinetics and cell quota values from samples in the western North Atlantic Ocean

Sample	Station	Latitude	Depth, m	Date	P_i, nM		V_{max}*, nM/h, amol·cell^{-1}·h^{-1}, pmol·cell^{-1}·h^{-1}	K_s, nM	R^2	α, V_{max}/K_s	Q_p†, nM, amol/cell, pmol/colony	V_{max}/Q_p, d^{-1}
1	BV46 20	39.7°N	5	10/2/11	0.5	Whole community	2.1	6.3	0.92	0.33	8	6.6
						Prochlorococcus	10.2	12	0.98	0.83	28	8.7
						Synechococcus	52	21	0.96	2.45	239	5.3
						Eukaryotes	121	26	0.95	4.60	1,743	1.7
2	BV46 BATS	31.7°N	5	10/6/11	0.5	Whole community	2.1	3.8	0.94	0.53	10	5.2
						Prochlorococcus	11.9	3.2	0.92	3.72	29	9.8
						Synechococcus	70	15	0.92	4.55	220	7.7
						Eukaryotes	77	41	0.95	1.86	6,474	0.3
3	BV46 12	21.7°N	5	10/13/11	0.5	Whole community	1.2	7.4	0.94	0.16	13	2.2
						Prochlorococcus	9.4	2.8	0.94	3.37	8	27.9
						Synechococcus	33	7.4	0.93	4.49	111	7.2
						Eukaryotes	475	185	0.91	2.57	4,198	2.7
						Trichodesmium	30	96	0.95	0.31	3	0.2
4	AE1206 Eddy	32.8°N	5	3/17/12	0.9	Whole community	1.5	16	0.93	0.10	16	2.3
						Prochlorococcus	1.3	3.4	0.93	0.38	—	—
						Synechococcus	5.6	2.5	0.93	2.29	—	—
						Eukaryotes	15.6	114	0.96	0.14	—	—
5	AE1206 BATS	31.7°N	5	3/19/12	0.7	Whole community	1.3	2.1	0.97	0.64	12	2.6
						Prochlorococcus	2.5	0.8	0.87	2.92	—	—
						Synechococcus	27	5.1	0.96	5.24	—	—
						Eukaryotes	70	177	0.96	0.40	—	—
6	AE1206 BATS	31.7°N	80	3/19/12	8	Whole community	0.13	26	0.97	0.005	15	0.2
						Prochlorococcus	1.2	32	0.97	0.04	—	—
						Synechococcus	1.2	24	0.95	0.05	—	—
						Eukaryotes	6.7	21	0.95	0.32	—	—
7	AE1319	55.0°N	5	8/25/13	150	Whole community	1.2	26.6	0.88	0.05	90	0.3
						Prochlorococcus	—	—	—	—	—	—
						Synechococcus	44	32.3	0.96	1.36	—	—
						Eukaryotes	76	51.5	0.98	1.47	—	—
8	AE1319	45.0°N	5	8/28/13	50	Whole community	1.2	30.4	0.96	0.04	37	0.8
						Prochlorococcus	—	—	—	—	—	—
						Synechococcus	38	38.4	0.99	0.99	—	—
						Eukaryotes	87	81	0.98	1.07	—	—
9	AE1319	39.0°N	5	9/3/13	0.5	Whole community	1.2	8.1	0.87	0.15	10	3.0
						Prochlorococcus	16	3.5	0.99	4.54	—	—
						Synechococcus	37	19	0.88	1.92	—	—
						Eukaryotes	9.6	17	0.97	0.55	—	—
10	AE1319 BATS	31.7°N	5	9/8/13	0.5	Whole community	2	4.5	0.98	0.44	10	4.9
						Prochlorococcus	16	4.4	0.98	3.66	—	—
						Synechococcus	119	9.9	0.96	12.00	—	—
						Eukaryotes	100	18	0.97	5.60	—	—
11	BV46 6	27.7°N	<25	10/9/11	0.5	*Trichodesmium*	28	639	0.98	0.04	2.3	0.3
12	BV46 8	25.7°N	<25	10/10/11	0.6	*Trichodesmium*	55	246	0.8	0.22	2.1	0.6
13	BV46 10	23.7°N	<25	10/11/11	0.4	*Trichodesmium*	17	142	0.92	0.12	1.6	0.3
Average values						Whole community	1.5 ± 0.6	12 ± 10	0.3 ± 0.2			
						Prochlorococcus	8.4 ± 6.4	3.8 ± 3.8	2.4 ± 1.7			
						Synechococcus	47 ± 34	17 ± 13	3.9 ± 3.4			
						Eukaryotes	115 ± 137	79 ± 67	2.0 ± 1.9			
						Trichodesmium	33 ± 16	342 ± 247	0.1 ± 0.1			

*The unit for V_{max} is nanomolar per hour for the whole community, attomoles per cell per hour for specific unicellular populations, and picomoles per colony per hour for *Trichodesmium*.
†The unit for Q_p is nanomolar for the whole community, attomoles per cell for specific unicellular populations, and picomoles per colony for *Trichodesmium*.

Table S2. Allometries used in the eco-evolutionary model and compilation of observed and model-emergent size and growth properties

	Model parameters				Observed and emergent behavior			
	a_K, nM	b_K	a_μ, d^{-1}	b_μ	Observed size, μm^3	Observed μ_{max}, d^{-1}	Emergent size range for $P_i < 20$ nM, μm^3	Emergent μ_{max}, d^{-1}
Prochlorococcus	3.98	0.30	0.75	−0.3	0.07	0.70	0.001–0.15	0.51
Synechococcus	3.98	0.30	3.00	−0.3	0.50	1.00	0.001–3.5	0.72
Picoeukaryotes	2.00	0.56	1.50	−0.2	8	0.6–1.2	0.001–22	0.58
Nanoeukaryotes	2.00	0.56	8.00	−0.2	180	0.6–1.8	0.001–280	1.35